Submitted to ADVANCED MATERIALS
DOI: 10.1002/adma.((please add manuscript number))

Anisotropic Thermal Transport in Thermoelectric Composites of Conjugated Polyelectrolytes / Single-Walled Carbon Nanotubes

By *Cheng-Kang Mai, Jun Liu,* Christopher M. Evans, Rachel A. Segalman, Michael L. Chabinyc, David G. Cahill,** and *Guillermo C. Bazan**

[*] Dr. C.-K. Mai, Prof. G. C. Bazan*
Center for Polymers and Organic Solids
Department of Chemistry and Biochemistry
University of California, Santa Barbara, CA 93117, USA
E-mail: bazan@chem.ucsb.edu
[*] Prof. Jun Liu
Department of Mechanical and Aerospace Engineering
North Carolina State University, Raleigh, NC 27695, USA
E-mail: jliu38@ncsu.edu
Dr. C. M. Evans, Prof. R. A. Segalman, Prof. M. L. Chabinyc
Departments of Chemical Engineering and Materials
University of California, Santa Barbara, CA 93106, USA
[*] Prof. D. G. Cahill
Department of Materials Science and Engineering and Materials Research Laboratory
University of Illinois, Urbana, IL 61801, USA
E-mail:d-cahill@illinois.edu

Keywords: Thermal conductivity, Anisotropy, Conjugated Polyelectrolyte, Carbon Nanotube, Thermoelectrics

Thermoelectrics comprise a renewable energy technology that converts heat directly to electricity without any moving parts. Organic thermoelectric materials, compared to their inorganic counterparts, have attracted attention because of several potential advantages,[1] including low toxicity, light weight, solution processablility, flexibility, low thermal conductivity, and tunable properties via chemical synthesis. The efficiency of thermoelectric devices is determined by the dimensionless figure of merit $ZT = \sigma S^2T/(\Lambda_e + \Lambda_{ph}) = S^2\Lambda_e /L(\Lambda_e + \Lambda_{ph}) = S^2 /L(1 + \Lambda_{ph}/\Lambda_e)$, where σ is the electrical conductivity, S is the Seebeck coefficient, T is the absolute temperature, Λ_e is the electronic component of the thermal conductivity, Λ_{ph} is the phonon contribution to the thermal conductivity, and L is the Lorenz number, $L = \Lambda_e/\sigma T$. Positive and negative S values correspond to predominant *p* and *n*-type charge transport, respectively. High performance thermoelectric materials should thus exhibit high S and small values of Λ_{ph}/Λ_e L.[21a] Recent developments on high performance PEDOT-

derived materials (*p*-type) have achieved *ZT* on the order of 0.1,[2] while developments on *n*-type thermoelectric materials remain more challenging. However, typical thermoelectric modules require both *p*- and *n*-type materials.[3]

Single-walled carbon nanotubes (SWNTs)[4] are one-dimensional prototype materials that are relevant for flexible electronics applications,[5] due to their ballistic charge transport,[6] excellent chemical stability[7] and mechanical strength.[8] Pristine SWNTs typically exhibit *p*-type charge transport from oxidation by air.[9] Complementary *n*-type composites can be obtained through doping with polyethyleneimine (PEI)[10] or small molecules with electron-rich units.[11] Although the thermal conductivity of an individual metallic SWNT has been measured to be on the order of 1000 W m^{-1} K^{-1},[12] what is observed in unaligned SWNT mats can be much lower (~ 30 W m^{-1} K^{-1}), presumably due to contact resistance between tubes or their bundled aggregates.[13] Because of the interaction of SWNTs with the organic matrix, SWNT/polymer composites typically exhibit low thermal conductivities that are similar to what is observed for polymers. SWNT/polymer composites have thus been recognized as materials that merit attention for the fabrication of flexible thermoelectric modules.[11b,14]

SWNT-based thermoelectric materials have been usually prepared as mats via filtration of SWNT dispersions mixed with surfactants and/or *n*-type dopants in polar solvents. Due to their large aspect ratios, SWNTs are likely to align along the in-plane direction during the filtration process, thus SWNTs are expected to exhibit anisotropic thermal transport. Because of the difficulty to access in-plane thermal conductivity of SWNT composites, through-plane thermal conductivity is often adopted for calculating *ZT* values, while σ and *S* are often measured along the in-plane direction.[15] Indeed, only a limited number of in-plane thermal conductivities of SWNT composites have been reported, which take advantage of steady-state thermal conductivity techniques.[14j] The full scope of how different composite contents, deposition conditions, influence of additives and the choice of

dopants impact anisotropic thermal conductivity in carbon nanotube composites remains to be fully understood.[16]

Conjugated polyelectrolytes (CPEs) can serves as SWNT dispersants.[17] The conjugated backbones of CPEs interact with the π-framework of SWNT walls, while the pendant ionic functionalities allow dispersion in polar solvents. Recently, it was reported that CPEs can selectively dope SWNTs to provide *p*- or *n*-type composites by the choice of pendant ionic functionalities (**Figure 1**).[18] Specifically, using the same π-conjugated backbone with cyclopenta-[2,1-b;3,4-b']-dithiophene-*alt*-4,7-(2,1,3-benzothiadiazole) (CPDT-*alt*-BT) repeat units, anionic CPEs (*i.e.* CPE-Na) and cationic CPEs (*i.e.* CPE-PyrBIm$_4$) provide *p*- and *n*-type conductive composites with single-walled carbon nanotubes. The combination of complementary doping and stable aqueous dispersions allows one to fabricate flexible thermoelectric devices via solution processing techniques. However, the thermal transport in these CPE/SWNT composites remains to be determined. In this contribution, we report the studies of CPE/SWNT composite films (both *p*- and *n*-type) as were prepared via vacuum filtration. Morphological details have been visualized by using scanning electron microscopy (SEM), and the anisotropy of thermal conductivity was determined by time-domain thermoreflectance (TDTR).[19]

The SEM images of top surfaces and cross-sections of both CPE-Na/SWNT and CPE-PyrBIm$_4$/SWNT films are shown in **Figure 2**. The cross sections of these films were prepared by freeze-fracture in liquid nitrogen. Comparison of Figure 2a-d shows that the broad morphological features for the two composites are very similar; switching the polarity of the charged groups pendant to the conjugated backbone thus plays a minor role in the structural organization, at least within the length scale of these SEM images. On the top surface (Figure 2a and 2c), one observes randomly aligned SWNT fibers (about 1-2 μm long), with the gaps filled with the polymer materials. It has been reported that the dispersion process by long time ultra-sonication can shorten the carbon nanotube.[20] However, when compared with the initial

materials, our results show that the length has not been significantly reduced. Dendritic-like structures can be observed in the cross section images in Figure 2b and 2d. Such morphology likely originated from the freeze-fracture process, which may have curved fibers previously aligned in the in-plane direction. These observations indicate that SWNTs have lower propensity to align along the through-plane direction and suggest that anisotropic thermal transport would be reasonable.

Samples prepared for thermal transport measurement need to be thicker than those used in previous studies that examined charge transport.[18] Therefore, we first verified that the same type of *p*- or *n*-doping dependence on CPE structure. Seebeck coefficient measurements showed that holes (positive *S*) and electrons (negative *S*) are the major charge carriers in CPE-Na/SWNT and CPE-PyrBIm$_4$/SWNT, respectively. Please refer to **Table 1** for a summary of the results. Consistent with previous reports, the *p*-type CPE-Na/SWNT (497 ± 74 S cm^{-1}) is more electrically conductive than the *n*-type CPE-PyrBIm$_4$/SWNT composite (32 ± 4 S cm^{-1}). For comparison, electrical conductivity of the spun-cast, neat CPE-Na film is measured to be 0.16 ± 0.01 S cm^{-1},[28a] while CPE-PyrBIm$_4$ is semiconducting.[28b] The same trend in therefore is observed when compared to the materials obtained through spin-coating.[18] One interesting conclusion is that the unusual doping dependence is resistant to changes in how the material is processed.

Thermal conductivities in both the through-plane and in-plane directions were measured by TDTR, a non-contact, pump-probe method.[19] This technique has been successfully used to measure the thermal conductivity of differently prepared PEDOT:PSS films,[21] which are the most commonly studied *p*-type organic thermoelectric materials.[22] For TDTR measurements, a mode-locked Ti:sapphire laser produces a train of pulses, which is divided into the pump and the probe beams. A mechanical delay stage is used to vary the relative optical path length between the pump and the probe beam before they are focused onto the sample surface through a single objective lens. The pump beam is modulated and

heats the sample surface, while the probe beam acts as a thermometer by detecting the change of surface reflectivity produced by the temperature change. Further details on TDTR can be found in previous publications.[19]

The conventional way to prepare the samples for TDTR measurements is to deposit metal transducer thin film (Al or AuPd) on top of the sample prior to acquiring data. The surfaces of both CPE/SWNT mats are, however, not sufficiently smooth for TDTR measurements. Atomic force microscopy (AFM) images of the top surfaces showed that the root mean square (rms) roughness (10 μm × 10 μm) is 154 nm and 121 nm for CPE-Na/SWNT and CPE-PyrBIm$_4$/SWNT composites, respectively (see Supporting Information). Typically, an rms roughness of < 15 nm in areas larger than the laser spot size (≈ 5 μm) is sufficient to avoid artifacts created by thermoelastic effects that modulate the intensity of diffuse light scattering. Therefore, we first sputtered the metal transducer thin film (AuPd, ~ 70 nm thick)[23] on a smooth glass substrate, and the CPE/SWNT mats on cellulose filter paper were attached to the metal surface with the aid of several drops of *iso*-propyl alcohol, followed by dipping the samples in acetone to dissolve the cellulose filter paper.[24] The two samples were deposited on the same substrate to minimize variations from the substrates. **Figure 3**c shows the sample configurations for through-plane thermal conductivity measurements. The pump and probe beams go through a transparent glass and focus at the AuPd/glass interface. Thus, the problem of beam reflection from a relatively rough surface of the mats is avoided. In such a sample configuration, heat flows bi-directionally, which is taken into consideration in the thermal diffusion model.

We first measured the through-plane thermal conductivity of poly(methyl methacrylate) (PMMA) to validate the TDTR measurement under this sample configuration.[21a,25] We fabricated a PMMA/AuPd/glass sandwich structure with 104 nm PMMA and 58 nm AuPd, and a control sample with the same AuPd/glass. Those samples were measured using a beam spot size with a width of w_o = 11.6 μm, and a modulation frequency of 9.2 MHz. The

thermal conductivity and heat capacity of AuPd used in our calculations can be found the literature.[23] The thickness of the AuPd layer was determined by picosecond acoustics using a sound speed velocity of 3.3 nm/ps. For the control sample, the thermal conductivity of the glass was measured as Λ = 1.19 W m^{-1} K^{-1} and the volumetric heat capacity was C = 2.15 J cm^{-3} K^{-1}. We then measured the thermal conductivity of PMMA in the sample configuration of PMMA/AuPd/glass, which is shown in **Figure 4**. The fitted thermal conductivity is Λ = 0.19 ± 0.02 W m^{-1} K^{-1}, which agrees well with the literature value of 0.18 - 0.20 W m^{-1} K^{-1}.[26]

The results for through-plane thermal conductivity measurements of CPE/SWNT composites are also shown in Figure 4, see also Table 1. The volumetric heat capacities were calculated by the density times the specific heat measured by modulated temperature differential scanning calorimetry (DSC), and at 298 K, they are C = 1.67 and 1.42 J cm^{-3} K^{-1} for both CPE-Na/SWNT and CPE-PyrBIm$_4$/SWNT, respectively. Therefore, the fitted thermal conductivity for these two samples were determined to be Λ = 0.16 ± 0.04 (CPE-Na/SWNT) and 0.14 ± 0.04 W m^{-1} K^{-1} (CPE-PyrBIm$_4$/SWNT). We found these results to be consistent in various locations, indicating relatively homogeneous mixing of CPEs and SWNTs in the micron scale. Note that these thermal conductivity data are comparable to previous reports on randomly packed polymer/SWNT composites (0.15 W m^{-1} K^{-1}).[14]

To measure the in-plane thermal conductivity of CPE/SWNT samples, we embedded the CPE/SWNT mats still with the filter paper into an epoxy matrix. The cross-sectional film surface was then prepared by dry-cutting the epoxy matrix parallel to the cross-sectional film direction using diamond blade ultramicrotomy. The same procedures have been successfully applied for PEDOT films.[21a] These samples were then oriented so that the direction of the incident laser beam is parallel to the original plane of the drop-cast film, as shown in Figure 3d. **Figure 5**a shows the CCD image of the sample surface with pump and probe beams after deposition of Al thin film. The relatively smooth region is much larger than the beam spot size (5.3 μm).

We measured the in-plane thermal conductivity using a 20× objective lens (w_o = 2.7 μm) at a modulation frequency of 9.2 MHz. The pump and probe power was carefully adjusted to make sure the steady state temperature rise is less than 30 K in the sample. Figure 5b shows the measurement data and the model fitting for both CPE-Na/SWNT (*p*-type) and CPE-PyrBIm$_4$ (*n*-type) samples. The acoustic echoes at 10-100 ps region were used to determine the Al film thickness. Thermal conductivity (Λ_{Al}) of Al thin film was calculated from the Wiedemann-Franz law ($\Lambda = L\sigma T$), where σ is the electrical conductivity of the same transducer layer deposited on a standard SiO_2 on Si sample, L is the *Lorenz* number (2.44 × 10^{-8} W Ω K^{-2}), and T is 298 K. We fitted the experiment data from 700 to 3600 ps, since from 100 to 700 ps, the strong thermoelastic effect in Al thin film makes the signal deviate from the thermal diffusion model. The interfacial thermal conductance between Al thin film and the CPE/SWNT sample was kept at G = 50 M W m^{-2} K^{-1}, as in previous work.[21a]

The in-plane thermal conductivities of CPE-Na/SWNT and CPE-PyrBIm$_4$/SWNT were determined to be 1.2 ± 0.2 and 1.6 ± 0.4 W m^{-1} K^{-1}, respectively. We repeated our measurements at different locations (many locations are sufficiently smooth for measurements as shown in the CCD image (Figure 5a)), and found that the thermal conductivity variations at different locations are within 15%. These experimental uncertainties and systematic uncertainties were combined to provide the total error bars. The systematic uncertainties of the thermal conductivity measurements are calculated by taking into account the individual uncertainties and sensitivities of the parameters in the thermal model. All the thermoelectric parameters of both CPE/SWNT composites are summarized in **Table 1**. Apparently, a large anisotropy was observed in these CPE/SWNT composites, and the anisotropic factors ($\Lambda_{thp}/\Lambda_{ip}$) were determined to be as large as 8 and 11 in CPE-Na/SWNT and CPE-PyrBIm$_4$/SWNT, respectively. Such anisotropies in thermal conductivity are usually observed in aligned carbon nanotube samples.[16] It has been hypothesized that phonon scattering at the carbon nanotubes junctions create large thermal contact resistance that reduces the thermal

conductivity of the composites down to the same order of organic polymers.[14e] Our results support that introducing CPEs into carbon nanotube is an effective method to lower the thermal conductivity of composites for suitable thermoelectric applications. But the anisotropy of the thermal conductivity in CPE/SWNT composites must be considered, and measured carefully in order to provide accurate *ZT* values.

All the thermal conductivity data (through-plane and in-plane) of these two composites are similar and significantly lower than that of individual carbon nanotube, although they exhibit very different electrical conductivities. In the absence of inelastic processes, the electron thermal conductivity can be estimated using Wiedemann−Franz relation, $\Lambda_e = L\sigma T$. Because the Lorenz number cannot be accurately determined, the exact value of Λ_e cannot be calculated. However, if we assume $L = 2.44 \times 10^{-8}$ W Ω K^{-2} and take the point of 298 K as an example, the in-plane electron thermal conductivities of CPE-Na/SWNT and CPE-$PyrBIm_4$/SWNT were estimated to be 0.36 and 0.023 W m^{-1} K^{-1}, respectively.[14e,27] The in-plane lattice thermal conductivity can be calculated then as 0.84 and 1.58 W m^{-1} K^{-1}, respectively. Apparently, phonon thermal conductivity in these two composites dominates the overall thermal transport. The Λ_e of CPE-$PyrBIm_4$/SWNT (1:1) is relatively smaller because of its lower σ, but the overall thermal conductivity is higher than that of CPE-Na/SWNT. Because CPE-$PyrBIm_4$/SWNT (1:1) has a higher SWNT volumetric fraction than CPE-Na/SWNT (1:1), as the molecular weight of CPE-$PyrBIm_4$'s repeat unit (1193.1 g mol^{-1}) is larger than that of CPE-Na (626.7 g mol^{-1}).

In conclusion, we report a method to measure the thermal conductivities of CPE/SWNT composites that are interesting within the context of simple to tune *p*- and *n*-type thermoelectric materials. Attaching the composites onto glass substrates with a pre-coated heat transducer allows one to measure the through-plane thermal conductivity of materials with rough surfaces by TDTR. The in-plane thermal conductivity can be measured by embedding thick samples into epoxy followed by microtoming to expose the relatively

smooth cross-sections. The thermal conductivity along the through-plane direction is found to be higher than that along the in-plane direction. Indeed, the anisotropy factor of thermal conductivity in these composites is approximately an order of magnitude, favoring in-plane direction. Such preferential transport in the in-plane direction should not be surprising given the large aspect ratio of carbon nanotubes and the preferential alignment of carbon nanotubes in the in-plane direction; however, the anisotropy value in the CPE/SWNT composites is now known quantitatively. These studies highlight the relevance of knowing the directional preference of thermal transport in organic composites when estimating *ZT* values from onlt through-plane thermoelectric measurements.

Experimental Section

Preparation of CPE/SWNT films: Purified arc discharge SWNTs (P2-SWNT) were purchased from Carbon Solutions, Inc. (Riverside, CA, USA) and used without further purification. CPE-Na and CPE-PyrBIm$_4$ were synthesized according to the literature [28]. Prior to filtration, a mixture of CPE/SWNT (1:1 weight ratio) in a solvent mixture of H_2O:MeOH (1:1 by volume, [SWNT] = 0.2 mg mL^{-1}) in an ice bath were subjected to probe sonication for 3 hours. The as-prepared dispersions were immediately filtered on top of a filter paper (cellulose, pore size is 0.45 μm) under vacuum. The thickness of the samples can be controlled by the initial volume of the dispersions. The as obtained CPE/SWNT mats (thickness > 50 μm) were dried under vacuum overnight in a chamber at 80□C, prior to morphology characterization and thermoelectric measurements. SEM images were obtained using an FEI XL30 Sirion FEG digital electron scanning microscope.

Measurements of □ and S: The σ values of CPE-Na/SWNT and CPE-PyrBIm$_4$/SWNT were measured via the four linear probe method as indicated in Figure 3a. This method eliminates the effects of contact resistance and avoids sample damage by sharp probes [2]. The uncertainties are determined from measurements of at least three different samples.

Seebeck coefficient measurements (Figure 3b) were performed in the same samples used to determine σ. The S values were determined by linear fitting of a series of measured thermovoltages by imposing a series of temperature differences across the sample ($S = -\Delta V/\Delta T$). Thermocouples were attached to the sample via a spring force from the probe arm, and good thermal contact was made with the thermal paste. The system was validated by measuring samples of bismuth telluride, silicon, and indium tin oxide, and the uncertainty was determined to be ±10−15% [29].

Acknowledgements
We acknowledge financial support from the AFOSR MURI FA9550-12-1-0002. The MRL Shared Experimental Facilities (SEM) are supported by the MRSEC Program of the NSF under Award No. DMR 1121053; a member of the NSF-funded Materials Research Facilities Network (www.mrfn.org).

Received: ((will be filled in by the editorial staff))
Revised: ((will be filled in by the editorial staff))
Published online: ((will be filled in by the editorial staff))

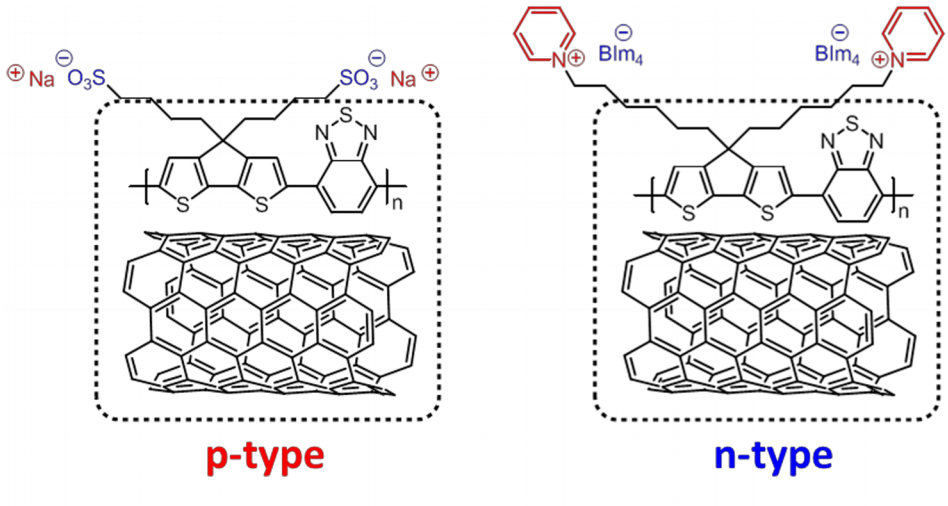

Figure 1. Chemical structures of CPE-Na and CPE-PyrBIm$_4$, which respectively provide *p*- and *n*-type thermoelectric composites, upon blending with single-walled carbon nanotubes. The dotted boxes indicate the hydrophobic interactions between the CPE conjugated backbone and the SWNT.

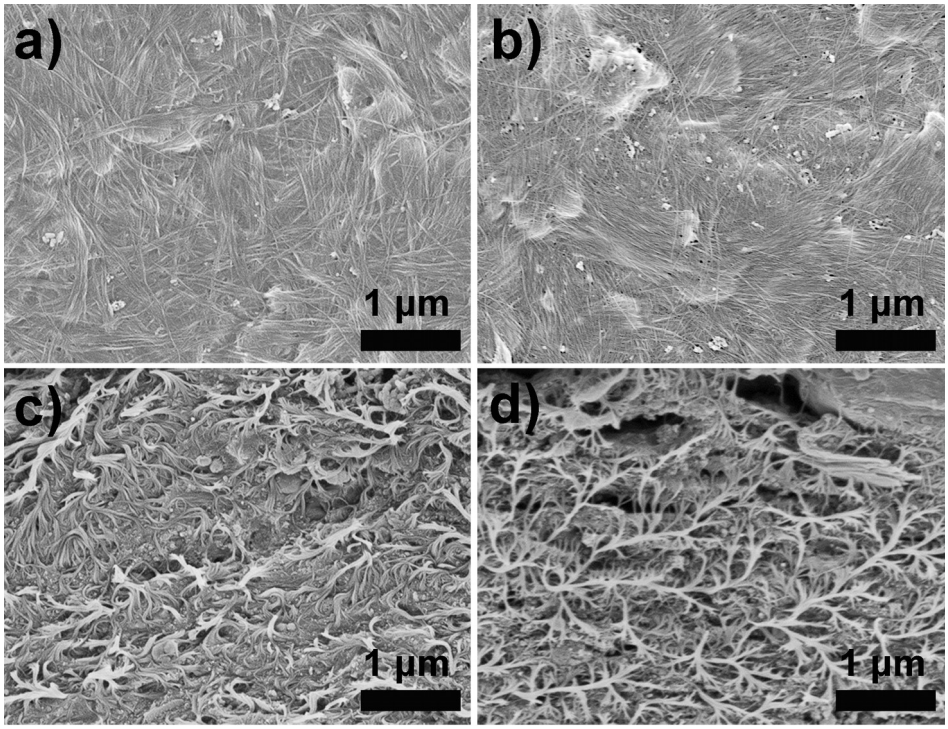

Figure 2. SEM images of CPE/SWNT composites, CPE-Na/SWNT (a: top surface, c: cross-section); CPE-PyrBIm$_4$/SWNT (b: top surface, d: cross-sections).

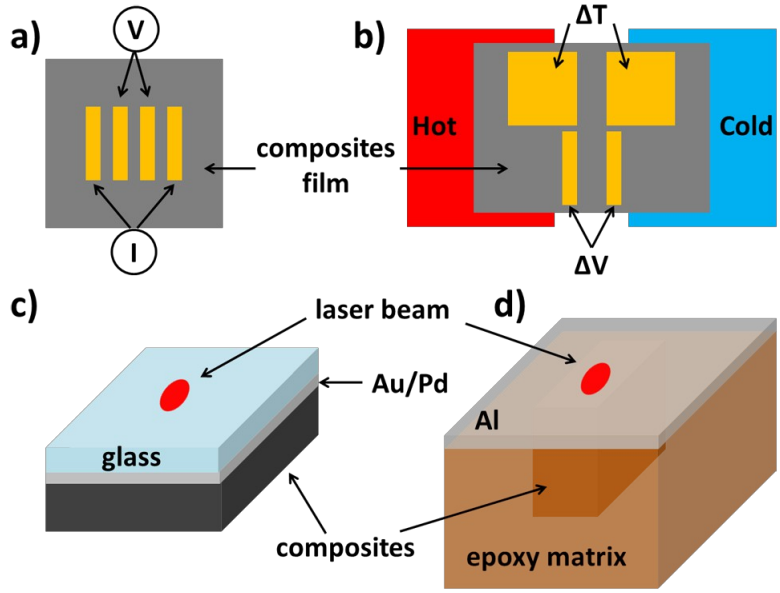

Figure 3. Schematic diagrams of thermoelectric characterizations of CPE/SWNT composite films. a) Electrical conductivity measurements using co-linear four-point-probe bar geometry; b) Seebeck coefficients are measured via the differential method, and calculated by linear fitting of a series of measured thermovoltages by imposing a series of temperature differences across the sample ($S = -\Delta V/\Delta T$); c) Sample configuration for through-plane thermal conductivity ($\Lambda_{\perp}$) measurements. Au/Pd is deposited on top of the glass substrate, prior to the attaching CPE/SWNT film. The incident laser beam is perpendicular to the plane of the glass substrate; d) Sample configuration for in-plane thermal conductivity ($\Lambda_{//}$) measurements. The CPE/SWNT films are embedded in an epoxy matrix, and the surfaces are exposed by diamond blade microtomy. Al thin films are deposited on top of the sample by magnetron sputtering. This sample was then oriented so that the direction of the incident laser beam is parallel to the original plane of the CPE/SWNT film.

Table 1. Thermoelectric parameters of both *p*- and *n*-type CPE/SWNT composites.[a]

Materials (weight ratio)	σ (S cm^{-1})	S (μV K^{-1})	Λ_{thp} (W m^{-1} K^{-1})[a]	Λ_{ip} (W m^{-1} K^{-1})[b]
CPE-Na/SWNT (1:1)	500 ± 70	46 ± 7	0.16 ± 0.04	1.2 ± 0.2
CPE-PyrBIm$_4$/SWNT (1:1)	32 ± 4	-73 ± 11	0.14 ± 0.04	1.6 ± 0.4

[a] Λ_{thp}: through-plane thermal conductivity; [b] Λ_{thp}: in-plan thermal conductivity.

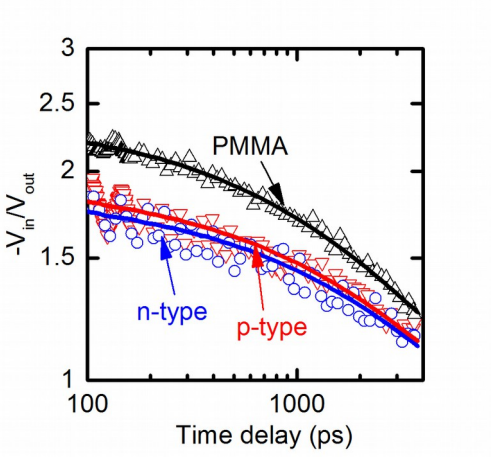

Figure 4. Data fitting for through-plane thermal conductivity of PMMA, CPE-PyrBIm$_4$/SWNT (*n*-type) and CPE-Na/SWNT (*p*-type) composite using AuPd transducer.

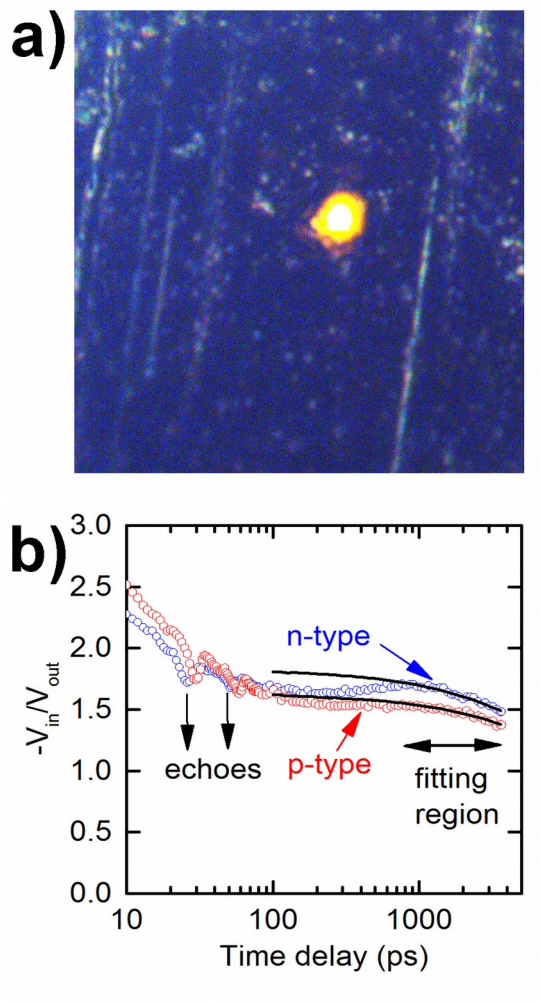

Figure 5. a) The CCD image of microtomed CPE-Na/SWNT sample surface with the pump and probe beam (yellow spot) after deposition of Al thin film and the diameter of the laser spot size is 5.3 μm; b) Data fitting for in-plane thermal conductivity of CPE-Na/SWNT (*p*-type, red) and CPE-PyrBIm$_4$/SWNT (*n*-type, blue) composites.

The table of contents entry

We report the anisotropic thermal conductivity of CPE/SWNT composite thick films (both *p*- and *n*-type) that were prepared via vacuum filtration. The thermal conductivity along the through-plane direction is found to be much higher than that along the in-plane direction, and the anisotropy factor of thermal conductivity in these composites is about an order of magnitude.

Keyword:
Thermal conductivity, Anisotropy, Conjugated Polyelectrolyte, Carbon Nanotube, Thermoelectrics

Authors:
Cheng-Kang Mai, Jun Liu,* Christopher M. Evans, Rachel A. Segalman, Michael L. Chabinyc, David G. Cahill,* and Guillermo C. Bazan*

Title:
Anisotropic Thermal Transport in Thermoelectric Composites of Conjugated Polyelectrolytes / Single-Walled Carbon Nanotubes

ToC figure

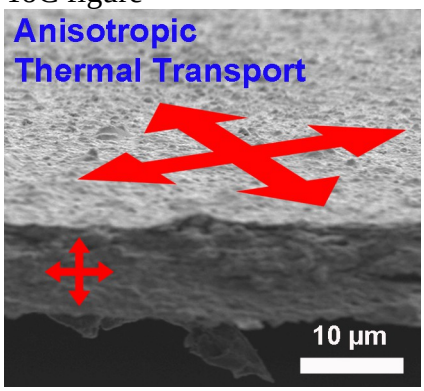

Supporting Information

Heat Capacity Measurements:

Density of the polymer films were determined by measuring the mass and volume of the material. The measured density is as follows: CPE-Na/SWNT: 1.55 g cm^{-3}, CPE-$PyrBIm_4$/SWNT: 1.69 g cm^{-3}. Specific heat capacity was measured using Perkin Elmer DSC 8000. The specific heat values were measured to be the following: CPE-Na/SWNT: 0.70 J g^{-1} K^{-1}; CPE-$PyrBIm_4$/SWNT: 0.61 J g^{-1} K^{-1}. Therefore, the volumetric heat capacity calculated are CPE-Na/SWNT: 1.09 J cm^{-3} K^{-1}; CPE- $PyrBIm_4$/SWNT: 1.03 J cm^{-3} K^{-1}.

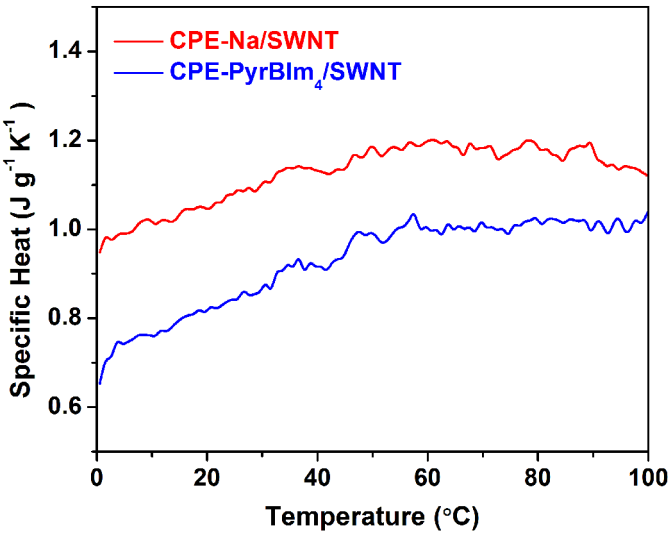

Figure S1. Specific heat measured by modulated temperature DSC.

Atomic Force Microscopy

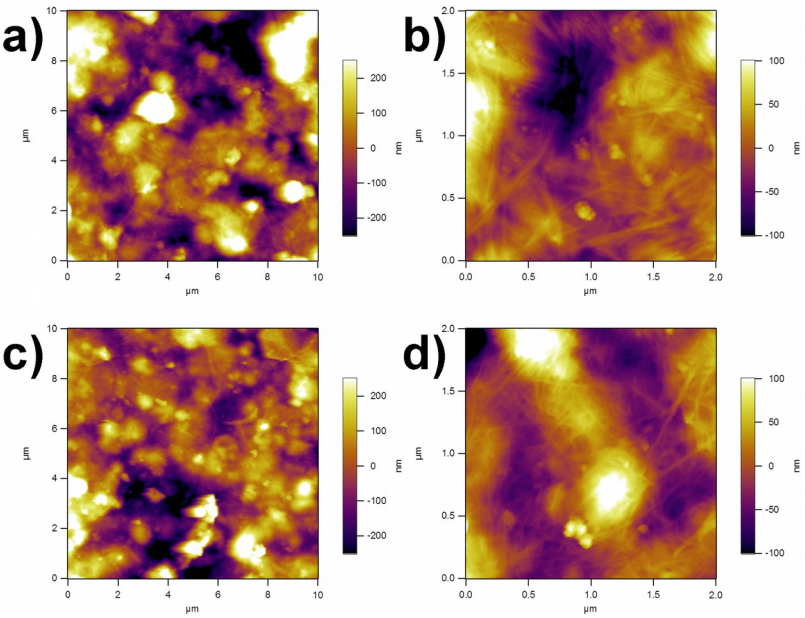

Figure S2. Surface topographic atomic force microscopy (AFM) images, CPE-Na/SWNT: a) 10 µm × 10 µm, root mean square (rms) roughness = 154 nm; b)) 2 µm × 2 µm, rms

roughness = 41 nm; CPE-PyrBIm4/SWNT: c) 10 μm × 10 μm, rms roughness = 121 nm; d) 2 μm × 2 μm, rms roughness = 43 nm.

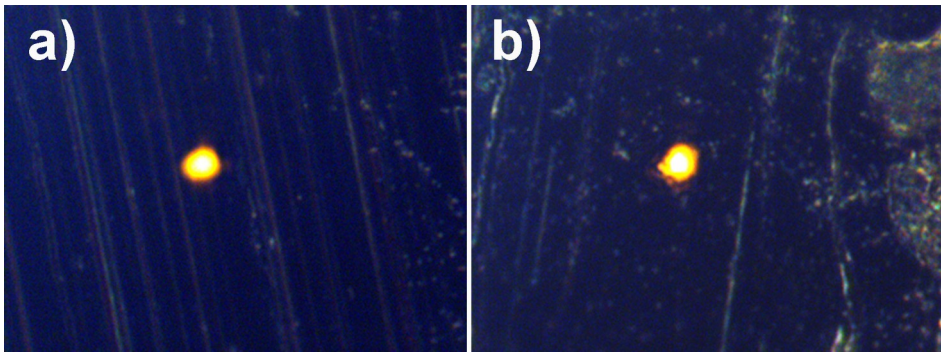

Figure S2. CCD images of microtomed sample surfaces for in-plane thermal conductivity measurements. The bright spot is the laser (diameter of the spot size is 5.3 um).

1_[]a) T. O. Poehler, H. E. Katz, *Energy Environ. Sci*. **2012**, *5*, 8110; b) N. Dubey, M. Leclerc, *J. Polym. Sci., Part B: Polym. Phys.* **2011**, *49*, 467; c) O. Bubnova, X. Crispin, *Energy Environ. Sci.* **2012**, *5*, 9345; d) Q. Zhang, Y. Sun, W. Xu, D. Zhu, *Adv. Mater.* **2014**, *26*, 6829; e) M. Culebras, C. Gómez, A. Cantarero, *Materials* **2014**, *7*, 6701; f) Y. Chen, Y. Zhao, Z. Liang, *Energy Environ. Sci.* **2015**, *8*, 401; g) B. T. McGrail, A. Sehirlioglu, E. Pentzer, *Angew. Chem. Int. Ed.* **2015**, *54*, 1710.

2_[]a) O. Bubnova, Z. U. Khan, A. Malti, S. Braun, M. Fahlman, M. Berggren, X. Crispin, *Nat. Mater.* **2011**, *10*, 429; b) G.-H. Kim, L. Shao, K. Zhang, K. P. Pipe, *Nat. Mater.* **2013**, *12*, 719; c) O. Bubnova, Z. U. Khan, H. Wang, S. Braun, D. R. Evans, M. Fabretto, P. Hojati-Talemi, D. Dagnelund, J.-B. Arlin, Y. H. Geerts, S. Desbief, D. W. Breiby, J. W. Andreasen, R. Lazzaroni, W. M. Chen, I. Zozoulenko, M. Fahlman, P. J. Murphy, M. Berggren, X. Crispin, *Nat. Mater.* **2014**, *13*, 190.

3_[]R. A. Schlitz, F. G. Brunetti, A. M. Glaudell, P. L. Miller, M. A. Brady, C. J. Takacs, C. J. Hawker, M. L. Chabinyc, *Adv. Mater.* **2014**, *26*, 2825; b) B. Russ, M. J. Robb, F. G. Brunetti, P. L. Miller, E. E. Perry, S. N. Patel, V. Ho, W. B. Chang, J. J. Urban, M. L. Chabinyc, C. J. Hawker, R. A. Segalman, *Adv. Mater.* **2014**, *26*, 3473; c) K. Shi, F. Zhang, C.-A. Di, T.-W. Yan, Y. Zou, X. Zhou, D. Zhu, J.-Y. Wang, J. Pei, *J. Am. Chem. Soc.* **2015**, *137*, 6979.

4_[]S. Iijima, *Nature* **1991**, *354*, 56.

5_[]a) C. Wang, K. Takei, T. Takahashi, A. Javey, *Chem. Soc. Rev.* **2013**, *42*, 2592; b) S. Park, M. Vosguerichian, Z. Bao, *Nanoscale*, **2013**, *5*, 1727.

6_[]S. Niyogi, M. A. Hamon, H. Hu, B. Zhao, P. Bhowmik, R. Sen, M. E. Itkis, R. C. Haddon, *Acc. Chem. Res.* **2002**, *35*,1105.

7_[]a) H. Dai, E. W. Wong, C. M. Lieber, *Science*, **1996**, *272*, 523; b) S. Tans, M. Devoret, H. Dai, A. Thess, *Nature*, **1997**, *386*, 474; c) K. S. Novoselov, A. K. Geim, S. V. Morozov, D. Jiang, Y. Zhang, S. V. Dubonos, I. V. Grigorieva, A. A. Firsov, *Science*, **2004**, *306*, 666.

8_[]a) M. M. J. Treacy, T. W. Ebbesen, J. M. Gibson, *Nature*, **1996**, *381*, 678; b) M. D. Lima, N. Li, M. J. de Andrade, S. Fang, S. J. Oh, G. M. Spinks, M. E. Kozlov, C. S. Haines, D. Suh, J. Foroughi,

S. J. Kim, Y. Chen, T. Ware, M. K. Shin, L. D. Machado, A. F. Fonseca, J. D. W. Madden, W. E. Voit, D. S. Galvão, R. H. Baughman, *Science*, **2012**, *338*, 928.

9_[]a) J. Kong, N. R. Franklin, C. Zhou, M. G. Chapline, S. Peng, K. Cho, H. Dai, *Science* **2000**, *287*, 622; b) P. G. Collins, *Science*, **2000**, *287*, 1801; c) K. Bradley, S. Jhi, P. Collins, J. Hone, M. Cohen, S. Louie, A. Zettl, *Phys. Rev. Lett.* **2000**, *85*, 4361.

10_[]M. Shim, A. Javey, N. W. Kam, H. Dai, *J. Am. Chem. Soc.* **2001**, *123*, 11512.

11_[]a) T. Takenobu, T. Takano, M. Shiraishi, Y. Murakami, M. Ata, H. Kataura, Y. Achiba, Y. Iwasa, *Nat. Mater.* **2003**, *2*, 683; b) Y. Nonoguchi, K. Ohashi, R. Kanazawa, K. Ashiba, K. Hata, T. Nakagawa, C. Adachi, T. Tanase, T. Kawai, *Sci. Rep.* **2013**, *3*, 3344.

12_[]E. Pop, D. Mann, Q. Wang, K. Goodson, H. Dai, *Nano Lett.* **2005**, *6*, 96.

13_[]J. Hone, M. C. Llaguno,, N. M. Nemes, A. T. Johnson, J. E. Fischer, D. A. Walters, M. J. Casavant, J. Schmidt, R. E. Smalley, *Appl. Phys. Lett.* **2000**, *77*, 666.

14_[] Review: a) C. A. Hewitt, D. L. Carroll, *Polymer Compoites for Energy Harvesting, Conversion, and Storage*, **2014**, ACS Symposium Series, ch. 9, vol. 1161, pp. 191–211; For selected examples: b) D. Kim, Y. Kim, K. Choi, J. C. Grunlan, C. Yu, *ACS Nano* **2010**, *4*, 513; c) Q. Yao, L. Chen, W. Zhang, S. Liufu, X. Chen, *ACS Nano* **2010**, *4*, 2445; d) W. Zhao, S. Fan, N. Xiao, D. Liu, Y. Y. Tay, C. Yu, D. Sim, H. H. Hng, Q. Zhang, F. Boey, J. Ma, X. Zhao, H. Zhang, Q. Yan, *Energy Environ. Sci.* **2012**, *5*, 5364; e) C. Yu, K. Choi, L. Yin, J. C. Grunlan, *ACS Nano* **2011**, *5*, 7885; f) J. Liu, J. Sun, L. Gao, *Nanoscale* **2011**, *3*, 3616; g) C. Yu, A. Murali, K. Choi, Y. Ryu, *Energy Environ. Sci.* **2012**, **5**, 9481; h) S. L. Kim, K. Choi, A. Tazebay, C. Yu, *ACS Nano* **2014**, *8*, 2377; i) N. Toshima, K. Oshima, H. Anno, T. Nishinaka, S. Ichikawa, A. Iwata, Y. Shiraishi, *Adv. Mater.* **2015**, *27*, 2246; j) H. Wang, J.-H. Hsu, S.-I. Yi, S. L. Kim, K. Choi, G. Yang, C. Yu, *Adv. Mater.* **2015**, *27*, 6855.

15_[] N. Toshima, K. Oshima, H. Anno, T. Nishinaka, S. Ichikawa, A. Iwata, Y. Shiraishi, *Adv. Mater.* **2015**, *27*, 2246.

16_[]a) Z. Han, A. Fina, *Prog. Polym. Sci.* **2011**, *36*, 914; b) A. M. Marconnet, M. A. Panzer, K. E. Goodson, *Rev. Mod. Phys*. **2013**, *85*, 1295.

17_[]a) S. K. Samanta, M. Fritsch, U. Scherf, W. Gomulya, S. Z. Bisri, M. A. Loi, *Acc. Chem. Res.* **2014**, *47*, 2446; b) Y. Li, C.-K. Mai, H. Phan, X. Liu, T.-Q. Nguyen, G. C. Bazan, M. B. Chan-Park, *Adv. Mater.* **2014**, *26*, 4697.

18_[]C.-K. Mai, B. Russ, S. L. Fronk, N. Hu, M. B. Chan-Park, J. J. Urban, R. A. Segalman, M. L. Chabinyc, G. C. Bazan, *Energy Environ. Sci.* **2015**, *8*, 2341.

19_[]D. G. Cahill, *Rev. Sci. Instrum.* **2004**, *75*, 5119.

20_[]a) W. Huang, Y. Lin, S. Taylor, J. Gaillard, A. M. Rao, Y.-P. Sun, *Nano Lett.* **2002**, *2*, 231; b) E. J. Weydemeyer, A. J. Sawdon, C.-A. Peng, *Chem. Commun.* **2015**, *51*, 5939.

21_[]a) J. Liu, X. Wang, D. Li, N. E. Coates, R. A. Segalman, D. G. Cahill, *Macromolecules* **2015**, *48*, 585; b) Q. Wei, M. Mukaida, K. Kirihara, T. Ishida, *ACS Macro Lett.* **2014**, *3*, 948.

22_[]Q. Wei, M. Mukaida, K. Kirihara, Y. Naitoh, T. Ishida, *Materials* **2015**, *8*, 732; b) R. Yue, J. Xu, *Synth. Met.* **2012**, *162*, 912.

23_[]W.-P Hsieh, D. G. Cahill, *J. Appl. Phys.* **2011**, *109*, 113520.

24_[]D. Sun, M. Y. Timmermans, Y. Tian, A. G. Nasibulin, E. I. Kauppinen, S. Kishimoto, T. Mizutani, Y. Ohno, *Nat. Nanotechnol.* **2011**, *6*, 156.

25_[]X. Wang, C. D. Liman, N. D. Treat, M. L. Chabinyc, D. G. Cahill, *Phys. Rev. B* **2013**, *88*, 075310.

26_[]a) S. A. Putnam, D. G. Cahill, B. J. Ash, L. S. Schadler, *J. Appl. Phys.* **2003**, *94*, 6785; b) M. J. Assael, S. Botsios, K. Gialou, I. N. Metaxa, *Int. J. Thermophys* **2005**, *26*, 1595.

27_[]W. Zhao, H. T. Tan, L. P. Tan, S. Fan, H. H. Hng, Y. C. F. Boey, I. Beloborodov, Q. Yan, *ACS Appl. Mater. Interfaces* **2014**, *6*, 4940.

28_[]a) C.-K. Mai, R. A. Schlitz, G. M. Su, D. Spitzer, X. Wang, S. L. Fronk, D. G. Cahill, M. L. Chabinyc, G. C. Bazan, *J. Am. Chem. Soc.* **2014**, *136*, 13478; b) Z. B. Henson, Y. Zhang, T.-Q. Nguyen, J. H. Seo, G. C. Bazan, *J. Am. Chem. Soc.* **2013**, *135*, 4163.

29_[]A. M. Glaudell, J. E. Cochran, S. N. Patel, M. L. Chabinyc, *Adv. Energy Mater.* **2014**, *5*, 140172.